Membrane curvature allosterically regulates the phosphatidylinositol cycle, controlling its rate and acyl-chain composition of its lipid intermediates

Received for publication, August 10, 2018, and in revised form, September 4, 2018 Published, Papers in Press, September 20, 2018, DOI 10.1074/jbc.RA118.005293

José Carlos Bozelli, Jr.[‡], William Jennings[‡], Stephanie Black[‡], Yu Heng Hou[‡], Darius Lameire[‡], Preet Chatha[‡], Tomohiro Kimura[‡], Bob Berno[§], Adree Khondker[¶‖1], Maikel C. Rheinstädter[¶‖], and Richard M. Epand[‡§2]

From the [‡]Department of Biochemistry and Biomedical Sciences, Health Sciences Centre, McMaster University, Hamilton, Ontario L8S 4K1 and the Departments of [§]Chemistry and [¶]Physics and Astronomy and the [‖]Origins Institute, McMaster University, Hamilton, Ontario L8S 4L8, Canada

Edited by Paul E. Fraser

Signaling events at membranes are often mediated by membrane lipid composition or membrane physical properties. These membrane properties could act either by favoring the membrane binding of downstream effectors or by modulating their activity. Several proteins can sense/generate membrane physical curvature (*i.e.* shape). However, the modulation of the activity of enzymes by a membrane's shape has not yet been reported. Here, using a cell-free assay with purified diacylglycerol kinase ϵ (DGKϵ) and liposomes, we studied the activity and acyl-chain specificity of an enzyme of the phosphatidylinositol (PI) cycle, DGKϵ. By systematically varying the model membrane lipid composition and physical properties, we found that DGKϵ has low activity and lacks acyl-chain specificity in locally flat membranes, regardless of the lipid composition. On the other hand, these enzyme properties were greatly enhanced in membrane structures with a negative Gaussian curvature. We also found that this is not a consequence of preferential binding of the enzyme to those structures, but rather is due to a curvature-mediated allosteric regulation of DGKϵ activity and acyl-chain specificity. Moreover, in a fine-tuned interplay between the enzyme and the membrane, DGKϵ favored the formation of structures with greater Gaussian curvature. DGKϵ does not bear a regulatory domain, and these findings reveal the importance of membrane curvature in regulating DGKϵ activity and acyl-chain specificity. Hence, this study highlights that a hierarchic coupling of membrane physical property and lipid composition synergistically regulates membrane signaling events. We propose that this regulatory mechanism of membrane-associated enzyme activity is likely more common than is currently appreciated.

The plethora of biological functions regulated by inositol phospholipids makes this lipid class one of the most important in cell physiology (1, 2). Although most of the signaling events are mediated through the interaction with their headgroups, it has been demonstrated in an increasing number of cases that lipid properties are dependent on the whole lipid structure, including the nature of their acyl-chains (3–8). Indeed, in mammals, inositol phospholipids are normally enriched with specific acyl-chains, namely 1-stearoyl-2-arachidonoyl acyl-chains (6, 7). The major metabolic pathway for the synthesis of phosphatidylinositol (PI)[3] and its phosphorylated forms is the PI cycle. This acyl-chain enrichment is in part accounted for by the specificity of the enzymes that catalyze steps within this cycle.

One of the steps of the PI cycle is the ATP-dependent phosphorylation of diacylglycerol (DAG) to produce phosphatidic acid (PA). In the cell, this reaction is catalyzed by diacylglycerol kinases (DGK). In mammals, there are 10 known DGK isoforms, and it has been proposed that DGKϵ is the isoform responsible for catalyzing this reaction within the PI cycle (9, 10). The enzyme when assayed *in vitro* using a mixture of phospholipid, detergent, and DAG (mixed micelles) exhibits a high degree of acyl-chain specificity for its DAG substrate, with 1-stearoyl-2-arachidonoyl glycerol (SAG) being the preferred substrate (11). Among all DGK isoforms, DGKϵ is the only one that bears this acyl-chain specificity, a property that was proposed to be due to the presence of an encoded conserved motif in the enzyme (12). These acyl-chains are the same as those found in inositol phospholipids. It has been proposed that this enrichment is in part due to the action of DGKϵ. Indeed, lipidomic studies showed that in mouse embryonic fibroblasts knocked out for DGKϵ, inositol phospholipids presented a decrease in the content

This work was supported by Canadian Natural Sciences and Engineering Research Council grant RGPIN-2018-05585 (to R. M. E.) and RGPIN-2016-06450 (to M. C. R.). This work was also supported by the Canada Foundation for Innovation (CFI), CIHR, and the Ontario Ministry of Economic Development and Innovation (to M. C. R.) and a University Scholar Award from McMaster University (to M. C. R.). The authors declare that they have no conflicts of interest with the contents of this article.

This article contains Table S1 and Figs. S1–S3.

[1] Recipient of a Canadian Institutes of Health Research (CIHR) undergraduate summer studentship award (Grant 153486).

[2] To whom correspondence should be addressed: Dept. of Biochemistry and Biomedical Sciences, McMaster University, Hamilton, Ontario L8S 4K1, Canada. Tel.: 905-525-9140 (ext. 22073); E-mail: epand@mcmaster.ca.

[3] The abbreviations used are: PI, phosphatidylinositol; DAG, diacylglycerol; DGK, diacylglycerol kinase(s); DGKϵ, ϵ isoform of DGK; DLS, dynamic light scattering; DO, 1,2-dioleoyl; DOG, 1,2-dioleoyl-*sn*-glycerol; DOPC, 1,2-dioleoyl phosphatidylcholine; DOPE, 1,2-dioleoyl phosphatidylethanolamine; ER, endoplasmic reticulum; H_{II}, inverted hexagonal; LUVs, large unilamellar vesicle; PA, phosphatidic acid; PE, phosphatidylethanolamine; PM, plasma membrane; PO, 1-palmitoyl-2-oleoyl; POPC, 1-palmitoyl-2-oleoyl phosphatidylcholine; POPE, 1-palmitoyl-2-oleoyl phosphatidylethanolamine; POPS, 1-palmitoyl-2-oleoyl phosphatidylserine; PS, phosphatidylserine; SAG, 1-stearoyl-2-arachidonoyl glycerol; MLV, multilamellar vesicle; Ni-NTA, nickel-nitrilotriacetic acid; ddH_2O, double-distilled H_2O.

of arachidonate, indicating the significant role of DGKε in enriching inositol phospholipids with this acyl-chain (10).

DGKε is the only isoform to be found permanently associated with a membrane. In a cell, it has been reported that the enzyme localizes to different membranes, *viz.* the plasma membrane (PM) and the endoplasmic reticulum (ER) (13, 14). Contrary to most metabolic cycles, steps of the PI cycle span two different locations (membranes) within a cell, the PM and ER, the same membranes where DGKε has been reported to be found. These two membranes have several different properties (*i.e.* lipid composition, thickness, and curvature). As DGKε lacks a putative regulatory domain, we hypothesized that either DGKε is constitutively active or it is regulated by the properties of the membrane it is bound to. To address this question, we chose to use a cell-free assay with purified DGKε and liposomes. This strategy allowed us to systematically vary the membrane properties while avoiding complications coming from other levels of regulation (proteins, metabolites, posttranslational modifications, etc.). Moreover, with 10 known DGK isoforms and no isoform-specific inhibitor available, addressing this question *in vivo* or in a cell-based assay would be challenging.

We demonstrate that both the specific activity and substrate acyl-chain specificity of DGKε are dependent on the shape of the membrane to which the protein binds. Only in highly curved membranes, such as those found in membrane fusion intermediates or at junctions between membranes of different morphologies, such as sheets and tubes, can the enzyme participate in the PI cycle. Our results indicate that this is not likely to occur in stable regions of either the ER or the PM, but rather at the junction between these two organelles where highly curved membrane structures have been reported.

Results

Marked differences in DGKε activity and acyl-chain specificity between mixed micelles and liposomes

Both the lipid substrate (DAG) and product (PA) of the DGKε-catalyzed reaction have low water solubility. Until now, DGKε activity assays have always been performed using mixed micelles (11, 15–17). However, these structures do not represent biological membranes, and it is difficult to systematically vary their physical properties. Using purified DGKε we can now, for the first time, assay the kinase activity and acyl-chain specificity in liposomes and compare the results with those using mixed micelles (Fig. 1).

In mixed micelles, purified DGKε activity as a function of DAG mol % showed Michaelis–Menten kinetics with clear differences between the enzyme's preferred substrate (SAG) and a nonpreferred substrate (1,2-dioleoyl-*sn*-glycerol; DOG), in agreement with the literature (Fig. 1*A*) (11, 18). For DGKε to catalyze the phosphorylation of DAG in liposomes, the enzyme must first translocate to the membrane. The purified enzyme spontaneously binds to liposomes (Fig. 1*B*). In the presence of 20 mol % 1-palmitoyl-2-oleoyl phosphatidylethanolamine (POPE), there is a ~5-fold increase in enzyme binding compared with POPC liposomes; however, there is little change in the specific activity of the enzyme. Evaluation of purified DGKε activity as a function of DAG mol % in 20 mol % POPE liposomes prepared as large unilamellar vesicles (LUVs) showed marked differences from mixed micelles (Fig. 1*C*). In this system, the enzyme also exhibited Michaelis–Menten kinetics; however, the activity and acyl-chain specificity were much lower than those observed in mixed micelles (note the difference in *y* axis scale).

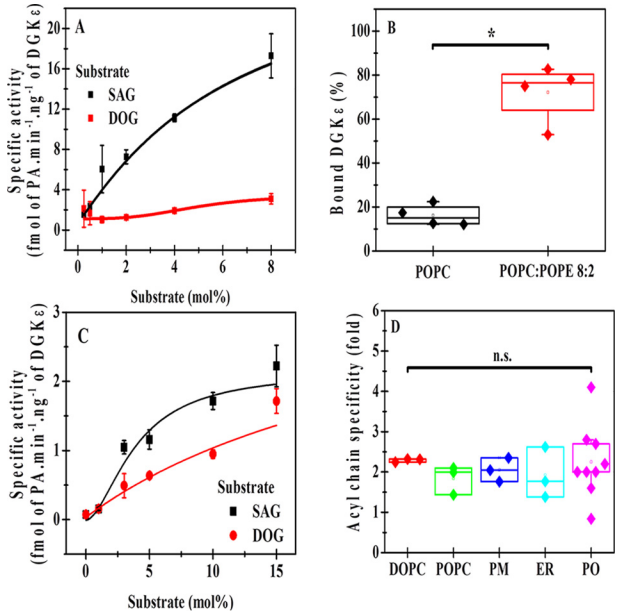

Figure 1. Marked differences in purified DGKε activity and acyl-chain specificity between mixed micelles and liposomes. *A*, specific activity of DGKε as a function of DAG mol % in mixed micelles. A comparison between the preferred substrate, SAG, and a nonpreferred substrate, DOG, is presented. Lipid composition was DOPC/DAG ((100 − *x*):*x*; mol/mol). Lipids were solubilized with 60 mM Triton X-100. The *lines* represent data fitting with Equation 2 to obtain the kinetic parameters (Table 1). *B*, comparison of the percentage of DGKε bound to liposomes made of two lipid compositions, POPC and POPC/POPE (8:2; mol/mol). Data are presented as a *box plot* including data of four independent experiments. *, $p < 0.01$. *C*, specific activity of DGKε as a function of DAG mol % in LUVs. A comparison between SAG and DOG is presented. Lipid composition was POPC/POPE/DAG ((80 − *x*):20:*x*; mol/mol/mol). The *lines* represent data fitting with Equation 2 to obtain the kinetic parameters (Table 1). *D*, acyl-chain specificity (the ratio between the activity for SAG and DOG, SAG/DOG; -fold) for liposomes with different lipid compositions (ER and PM bear a lipid mixture comprising the major phospholipids found in those membranes at their respective molar ratio. PO refers to POPC/POPE/DAG (30:60:10; mol/mol/mol)). Data are presented as a *box plot* including data of three independent experiments for all lipid compositions, except PO, for which data of nine independent experiments are presented. *n.s.*, not significant. These results were obtained using a final total lipid concentration of 5 mM at pH 7.2. Data in *A* and *C* are presented as mean ± S.D. (*error bars*) and are representative of three independent experiments.

To quantitatively assess the differences observed between the mixed micelles and liposomes, we calculated the kinetic parameters K_m (the Michaelis–Menten constant, which is a measure of the dissociation constant of the enzyme–substrate complex), k_{cat} (the catalytic rate constant, which is a measure of the enzyme turnover), and k_{cat}/K_m (the pseudo-first order rate constant at low substrate concentration, which is a measure of the enzyme catalytic efficiency) for SAG and DOG (Table 1). In mixed micelles, the data showed similar values of K_m for SAG and DOG, whereas k_{cat} and k_{cat}/K_m were found to be about 5-fold and 7-fold higher, respectively, for SAG compared with DOG. These results suggest that in mixed micelles, the enzyme has a similar affinity for both substrates. However, it converts

Table 1

Comparison of the the kinetic parameters of purified DGKε between mixed micelles and liposomes

K_m is the Michaelis–Menten constant (mol %). k_{cat} is the catalytic rate constant (s^{-1}). k_{cat}/K_m is the pseudo-first order rate constant at low substrate concentrations (s^{-1} mol $\%^{-1}$). These parameters were obtained by the fitting of the corresponding kinetic curves with Equation 2. The results are presented as the mean ± S.E. ($n = 3$).

Lipid carrier	Substrate	K_m	k_{cat}	$k_{cat/Km}$
		mol %	s^{-1}	s^{-1} *mol* $\%^{-1}$
Mixed micelles	SAG	4 ± 1	23 ± 4	7.0 ± 1.3
	DOG	5 ± 1	5 ± 1	1.0 ± 0.3
Liposomes	SAG	6 ± 1	3 ± 1	0.4 ± 0.2
	DOG	18 ± 3	3 ± 1	0.2 ± 0.1

SAG into product more rapidly than DOG, in agreement with previous results (11, 18).

In LUVs, the data yielded K_m values on average 3-fold smaller for SAG compared with DOG, showing that the enzyme bears increased affinity for SAG over DOG (Table 1). However, the enzyme turnover (k_{cat}) was found to be similar between both substrates and ~8-fold smaller when compared with the values found in mixed micelles when SAG was used as a substrate. These results showed a lower enzymatic activity and no large acyl-chain specificity in LUVs. As a result of a considerably smaller k_{cat}, the catalytic efficiency (k_{cat}/K_m) was found to be ~23-fold smaller than that observed for mixed micelles when SAG was the substrate.

The marked differences in kinase activity between mixed micelles and liposomes suggested that DGKε is weakly active and bears no large acyl-chain specificity in a cell membrane. Hence, we decided to evaluate whether the low activity and acyl-chain specificity depended on the lipid composition. We measured the enzyme activity and acyl-chain specificity for a variety of lipid compositions from simple ones (DOPC, POPC, and POPC/POPE (1:2)) to more complex ones (mixtures of six or seven lipids chosen to represent the lipid composition of the ER or the PM membranes at their respective molar ratio (19)). The results showed that the enzyme presents low activity (not shown) and acyl-chain specificity (Fig. 1*D*) regardless of the liposome composition. These data suggested that the enzyme is weakly active and lacks acyl-chain specificity in a cell membrane regardless of its lipid composition.

Membrane global morphological changes enhance DGKε kinase activity and acyl-chain specificity

As the lipid composition does not modulate DGKε activity and acyl-chain specificity, we decided to further investigate whether other membrane properties could regulate the enzyme function. The preferred binding of DGKε to PE-containing liposomes suggested that PE might play a role in DGKε activity and acyl-chain specificity. To evaluate the effect of PE on the kinase activity of purified DGKε, we measured the enzyme activity in LUVs as a function of PE mol % for two molecular species of PE, namely POPE and 1,2-dioleoyl phosphatidylethanolamine (DOPE), using their phosphatidylcholine counterparts as the host lipid (POPC and DOPC). These two PE molecular species bear different intrinsic tendencies to bend (20). Hence, if membrane intrinsic curvature plays a role in DGKε activity, we would observe divergent lines as we increase the mol % of POPE versus DOPE (21).

The activity of the enzyme was essentially constant, and the curves for both PE molecular species were overlapped as we increased the PE content from 0 to 45 mol %, indicating that membrane intrinsic curvature does not play a role in DGKε activity (Fig. 2*A*). However, at 60 mol % PE, an 18-fold increase in DGKε activity was observed for liposomes prepared with lipids bearing 1,2-dioleoyl (DO) acyl-chains compared with lipids bearing 1-palmitoyl-2-oleoyl (PO) acyl-chains. To better understand the mechanism of this large increase in DGKε activity, we first measured the binding of the enzyme to liposomes prepared with 60 mol % POPE (Fig. 2*B*). We did not succeed in measuring the enzyme binding to liposomes prepared with 60 mol % DOPE because this lipid mixture could not readily be separated from the aqueous phase by centrifugation. The results with the 60 mol % POPE lipids showed that on average, 62% of the enzyme was bound when SAG was the substrate and ~3-fold less when DOG was the substrate. The fact that a large fraction of the enzyme was bound when SAG was the substrate suggested that the lower activity observed with 60 mol % POPE compared with DOPE cannot be accounted for by only a difference in membrane binding of the enzyme.

Intrinsic curvature refers to the curvature a lipid monolayer would acquire if it was not constrained to be a bilayer. The term "negative" is an arbitrary term used to distinguish the curvature in which the monolayer curves around the lipid headgroup from the opposite type of curvature (*i.e.* "positive"), in which the monolayer curves around the lipid acyl-chain. As a measure of the membrane intrinsic negative curvature, the lamellar-to-hexagonal phase transition temperature for DOPE is ~4 °C, whereas that for POPE is ~70 °C (22). Hence, we hypothesized that the large content of DOPE (60 mol %) in the sample could lead to a physical membrane bending, resulting in a change of morphology of the lipid aggregate. This change in shape of the model membrane could explain the observed differences in enzyme activity. Dynamic light scattering (DLS) measurements showed that the 60 mol % POPE sample had a hydrodynamic diameter of ~92 nm, which was determined by the extrusion procedure of sample preparation. In contrast, the 60 mol % DOPE sample, even after 10 cycles of extrusion, presented lipid aggregates with a hydrodynamic diameter ranging from 700 to 1750 nm (Fig. S1). These data suggested that the 60 mol % DOPE sample changed the lipid aggregated morphology from a lipid vesicle to a large, aggregated inverted phase. To evaluate this, we studied phase behaviors of these lipid systems by acquiring their static ^{31}P NMR spectra. Measurements of the static ^{31}P NMR powder patterns provide a well-established method to assess the shapes of membrane phases (23). The static ^{31}P NMR spectrum of the 60 mol % POPE aqueous dispersion sample showed a powder pattern with intense peaks in the upfield region (Fig. 2*C*). This spectral line shape is characteristic of lipids assembled as a lamellar phase (bilayer), which represents a locally flat membrane in relation to the size of the enzyme and its membrane binding platform. On the other hand, the static ^{31}P NMR spectrum of the 60 mol % DOPE sample showed a mixture of different types of overlapping powder patterns containing intense isotropic and downfield peaks along with upfield peaks corresponding to the lamellar phase (Fig. 2*D*). The presence of the powder patterns with the isotro-

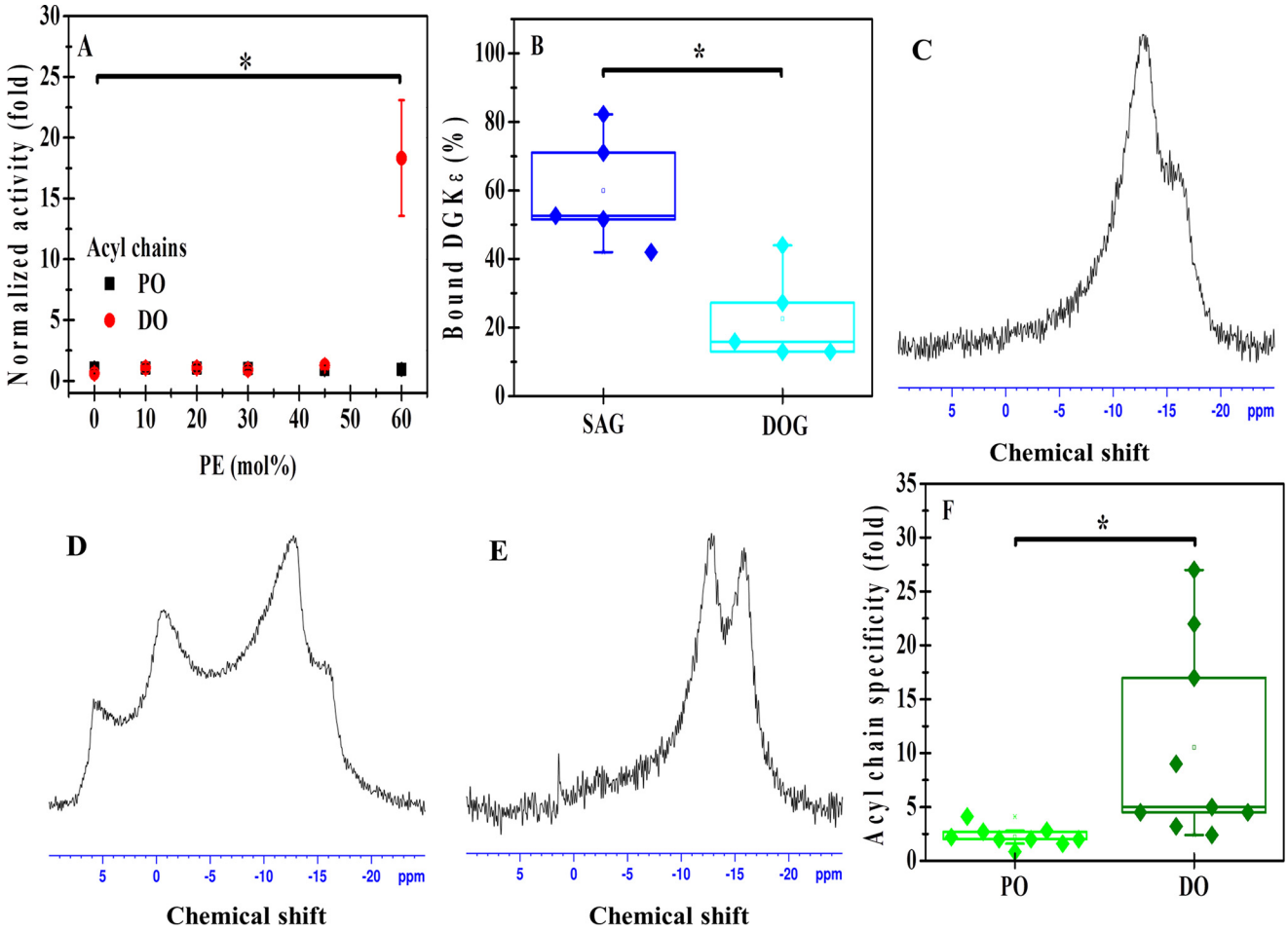

Figure 2. Membrane global morphological changes enhance purified DGKε kinase activity and acyl-chain specificity. *A*, normalized activity of DGKε as a function of PE mol %. The experiments were performed using two lipid compositions, POPC/POPE/SAG ((90 − *x*):*x*:10; mol/mol/mol) and DOPC/DOPE/SAG ((90 − *x*):*x*:10; mol/mol/mol) ($n = 3$ for 0–45 mol % PE and $n = 12$ for 60 mol % PE; mean ± S.E.; *, $p < 0.01$). *B*, percentage of DGKε bound to liposomes. *SAG*, POPC/POPE/SAG (30:60:10; mol/mol/mol); *DOG*, POPC/POPE/DOG (30:60:10; mol/mol/mol). Data are presented as a *box plot* including data of four independent experiments. *, $p < 0.01$. Shown are ^{31}P NMR spectra of MLVs in solution: POPC/POPE/SAG (30:60:10; mol %) (*C*), DOPC/DOPE/SAG (30:60:10; mol %) (*D*), and DOPC/DOPE/SAG (45:45:10, mol %) (*E*). Spectra were acquired at 25 °C. *F*, acyl-chain specificity (the ratio between the activity for SAG and DOG, SAG/DOG, -fold) for POPC/POPE/DAG (30:60:10; mol/mol/mol) and DOPC/DOPE/DAG (30:60:10; mol/mol/mol). Data are presented as a *box plot* including data of nine independent experiments. *, $p < 0.01$. Total lipid concentration on activity and binding assays was 5 mM, and the concentration for ^{31}P NMR experiments was 65 mM. Experiments were carried out at pH 7.2.

pic and downfield peaks evinced the presence of highly curved nonlamellar structures in this sample as we expected. The isotropic and downfield peaks are ascribed to bicontinuous cubic and inverted hexagonal (H_{II}) phases, respectively (23). Finally, to test whether the lack of enhancement in activity was because of the absence of highly curved nonlamellar structures, we acquired static ^{31}P NMR of the aqueous dispersion of the 45 mol % DOPE sample, for which we did not observe changes in enzymatic activity (Fig. 2*A*). Indeed, the spectrum showed a powder pattern typical of a lamellar phase (Fig. 2*E*). These results indicated that the enzyme has low enzymatic activity in the presence of locally flat bilayers and that the presence of the highly curved structures greatly enhances its activity.

The finding that highly curved membranes greatly enhanced DGKε activity led to the question whether this would also enhance its acyl-chain specificity, an important property for its function within the PI cycle. In Fig. 2*F*, we compare the enzyme acyl-chain specificity between a locally flat (60 mol % POPE) and a highly curved (60 mol % DOPE) membrane. The data showed that the acyl-chain specificity was increased on average 11-fold in the presence of highly curved nonlamellar structures (60 mol % DOPE) compared with locally flat membranes (60 mol % POPE). It is important to mention that the lipid morphology of the 60 mol % PE samples were qualitatively similar regardless of whether the substrate was SAG or DOG based on their static ^{31}P NMR spectra (Fig. 2*C* and Fig. S2*A* for 60 mol % POPE and Fig. 2*D* and Fig. S2*B* for 60 mol % DOPE). This result demonstrates that different DAGs do not markedly affect the membrane morphology. Therefore, it is the presence of highly curved membrane structures on the 60 mol % DOPE sample that endow DGKε with the ability to discriminate the nature of the acyl-chain of its lipid substrate.

We also monitored the role of membrane curvature by using liposomes of varied size. The spherical shape of liposomes means that the outer monolayer has positive mean curvature. The liposomes also have the shape of a sphere, which means that the Gaussian curvature is also positive (*i.e.* the curvatures at right angles to each other have the same signs). As the liposomes get smaller, the outer monolayer to which the enzyme binds acquires greater positive mean as well as Gaussian curva-

tures. This results in lower activity of DGKε (Table S1). DOPE is a lipid with strong intrinsic negative curvature, and the results presented above showed that greater negative membrane curvature supports higher enzyme activity. The results with LUVs of different sizes show that positive curvature has the opposite effect on enzyme activity (*i.e.* inhibition), independently supporting the conclusion of high curvature as a mechanism to modulate DGKε activity.

DGKε presents enhanced activity and acyl-chain specificity in a pure cubic phase

As shown above, the DGKε activity and acyl-chain specificity are markedly increased in the presence of highly curved nonlamellar structures. However, the morphology of the 60 mol % DOPE sample was fairly complex based on the static ^{31}P NMR spectrum with the presence of a cubic and hexagonal phase in addition to the lamellar one. Hence, we decided to further investigate whether these properties of activity and acyl-chain specificity also increased in lipids having only a single inverted phase with cubic or hexagonal symmetry. A comparison of enzyme activity between DOPE (H_{II} phase) and DOPC (lamellar phase) showed no large differences in the low kinase activity observed (not shown).

We then compared the activity of the enzyme between a locally flat membrane and a pure cubic phase. It is known that DAG can induce a bilayer-to-cubic phase transition in certain conditions (24). Because the 60 mol % DOPE sample presented a cubic phase component, we attempted to fully transition this sample to a pure cubic phase by thermal cycling. The static ^{31}P NMR spectrum of the 60 mol % DOPE sample after being heated at 70 °C for 10 min and recooled to room temperature is presented in Fig. 3*A*. The spectrum is a single isotropic peak, consistent with the lipid being a pure cubic phase. However, there are other structures that could give rise to an isotropic peak in the ^{31}P NMR spectrum, such as small lipid aggregates and/or micelles. Hence, to confirm the presence of a cubic phase in this sample, we employed small-angle X-ray diffraction (Fig. 3*B*). The two-dimensional reciprocal space map of this sample is presented in the *top panel*. The diffraction data are characterized by a pattern of diffraction lines indicating a cubic phase with Pn3m symmetry (*bottom panel*). There are no other diffraction lines, in agreement with the ^{31}P NMR that showed a single isotropic peak. It is important to mention that this version of a cubic phase has been associated with membrane fusion events (25).

A comparison of the DGKε kinase activity in the presence of 60 mol % POPE and 60 mol % DOPE is presented in Fig. 3*C*. For the latter, a fresh sample was compared with one that had been heated to 70 °C for 10 min, which we showed by NMR and X-ray diffraction is a pure cubic phase. The data showed that the enzyme is able to catalyze its reaction in a pure cubic phase. Most importantly, when compared with a locally flat bilayer (60 mol % POPE) the activity was on average 9-fold higher in the pure cubic phase (heated 60 mol % DOPE). This large increase in activity is not caused by an increase in accessibility of the enzyme to the lipid surface, as there is a ~2-fold difference in activity measured using multilamellar vesicles (MLVs) compared with extruded LUVs (not shown). In addition, our DLS measurements indicate that the LUVs are indeed mostly unilamellar, and hence conversion to the cubic phase would not result in close to an order of magnitude increase in activity due to greater accessibility of the enzyme to the lipid surface in a cubic phase. These results showed that in a pure cubic phase, which presents highly curved membranes, the enzyme enhances its activity compared with a locally flat bilayer to values similar to those observed in the 60 mol % DOPE sample, which was the highest value measured. In addition to its higher activity in a pure cubic phase, the enzyme also retains acyl-chain specificity similar to those found for the fresh 60 mol % DOPE sample, which is the system with the highest acyl-chain specificity measured (Fig. 3*D*).

DGKε kinase activity and acyl-chain specificity are enhanced at sites of membrane fusion intermediates

Our finding that DGKε retains its maximally observed activity and acyl-chain specificity in a pure cubic phase led us to investigate the likely biological relevance of this result. Recently, the high-resolution structure of cubic phases has been resolved by cryo-EM tomography (26). The interface of this structure resembles intermediates that are often associated with membrane fusion phenomena (27, 28). In addition, cubic phase with Pn3m symmetry has been associated with membrane fusion events (25). Hence, we designed an experiment to evaluate whether the presence of membrane fusion intermediates could enhance DGKε kinase activity as well as its acyl-chain specificity.

To address this question, we measured DGKε kinase activity and acyl-chain specificity using a widely studied system of membrane fusion (*i.e.* the Ca^{2+}-induced fusion of phosphatidylserine (PS)-containing liposomes) (29, 30). As a control, we measured the addition of Ca^{2+} to liposomes in the absence of PS. The results did not show any enhancement in enzyme activity (Fig. 4*A*, 0 PS) or acyl-chain specificity (Fig. 4*B*, 0 PS) in liposomes without PS, showing that Ca^{2+} by itself cannot account for changes in activity and acyl-chain specificity of the enzyme, as expected because of the absence of a Ca^{2+}-binding motif in DGKε structure. However, when the liposomes presented 40 mol % PS, incubation with Ca^{2+} before the activity assays led to, on average, a 19-fold enhancement of DGKε kinase activity (Fig. 4*A*, 40 mol % PS) and an 8-fold enhancement of acyl-chain specificity (Fig. 4*B*, 40 mol % PS). These values are similar to those observed for the 60 mol % DOPE sample and clearly showed that membrane fusion intermediates are sites of maximum DGKε kinase activity and acyl-chain specificity.

DGKε promotes membrane morphological changes

Finally, we studied whether the interaction of DGKε with membranes induces morphological changes, based on measurements of static ^{31}P NMR of the aqueous dispersion of the lipid systems in the absence or presence of DGKε (1:10,000 protein/lipid molar ratio). The lipid systems studied were 60 mol % POPE (locally flat membrane) and 60 mol % DOPE (highly curved membrane) with SAG (Fig. 5) or DOG (Fig. S3).

The data showed that regardless of the substrate, the enzyme induced little or no change in a locally flat bilayer (60 mol %

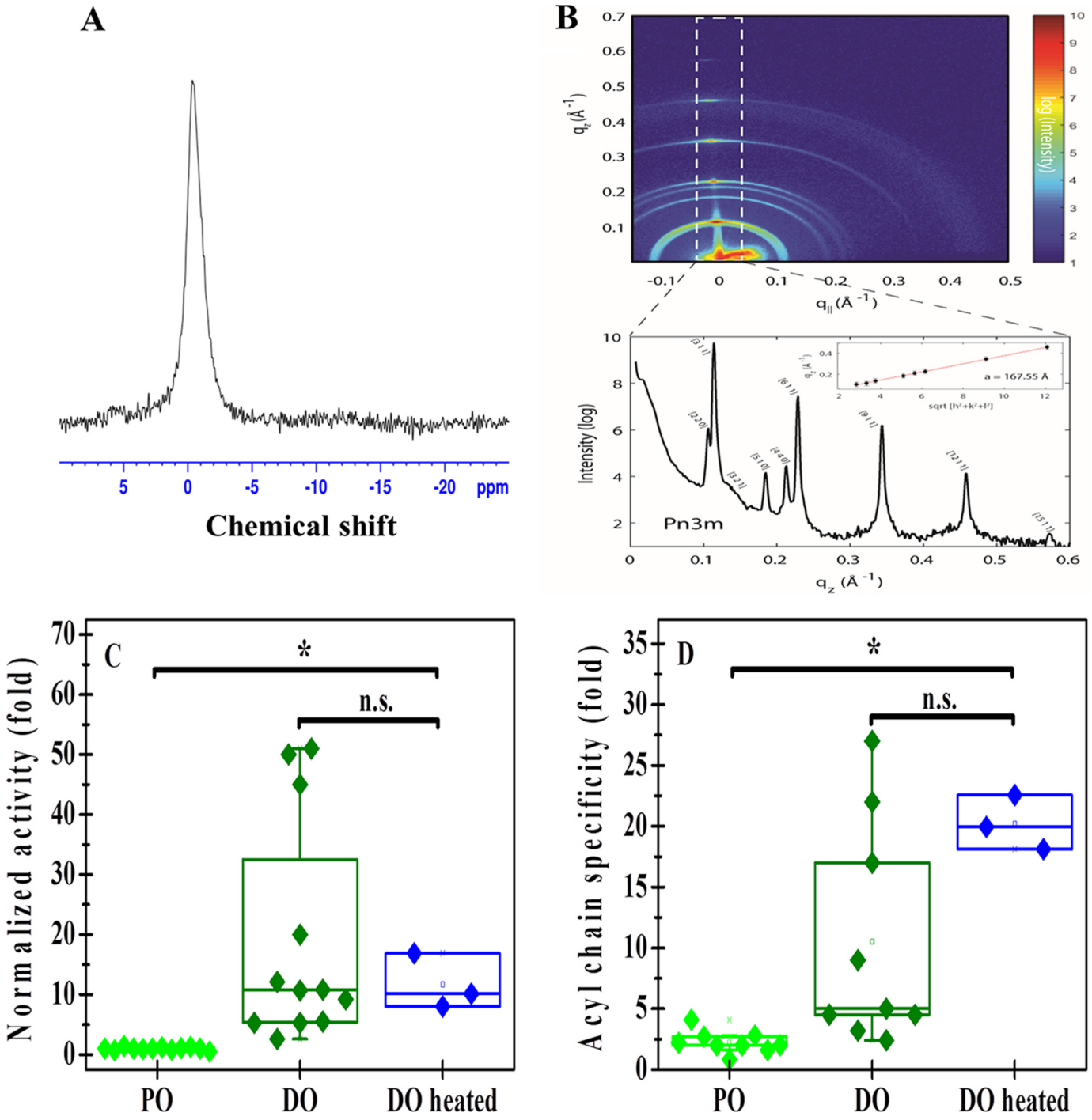

Figure 3. DGKε presents enhanced activity and acyl-chain specificity in a pure cubic phase. *A*, ^{31}P NMR spectra of 65 mM DOPC/DOPE/SAG (30:60:10; mol/mol/mol) after heating the sample for 10 min at 70 °C. The spectrum was acquired at 25 °C. *B*, X-ray diffraction of the same sample. *Top*, two-dimensional X-ray data. *Bottom*, plot as a function of scattering vector q_z. The *inset* shows that the peak positions are consistent with the symmetry elements of a Pn3m phase. The quality of the peak assignments is shown by the perfectly linear behavior. Data were acquired at 30 °C. The calculated lattice parameter and water channel diameter were 16.8 and 9.3 nm, respectively. *C* and *D*, normalized kinase activity of DGKε (*C*) and DGKε acyl-chain specificity (*D*) (the ratio between the activity for SAG and DOG (SAG/DOG), -fold) as a function of lipid composition. *PO*, POPC/POPE/SAG (30:60:10; mol/mol/mol); *DO*, DOPC/DOPE/SAG (30:60:10; mol/mol/mol); *DO heated*, DO sample after heating the sample for 10 min at 70 °C. Data are presented as a *box plot*. For DO heated, data of three independent experiments are presented. For DO and PO, data of 12 and 9 independent experiments are presented for activity and acyl-chain specificity, respectively. *, $p <$ 0.01; *n.s.*, not significant at 0.05 level. Experiments were carried out at pH 7.2.

POPE; Fig. 5*A* and Fig. S3*A*). However, in the 60 mol % DOPE sample, which presents highly curved nonlamellar structures, the enzyme induced large morphological changes even in a protein/lipid molar ratio as low as 1:10,000 (Fig. 5*B* and Fig. S3*B*). In the presence of the enzyme, normalization to the isotropic peak showed a relative decrease in both the downfield peak and the upfield peaks in the sample with the enzyme. These results showed that in systems that have the propensity to form the cubic phase, which bears highly curved nonlamellar structures, the enzyme favors the formation of this membrane structure,

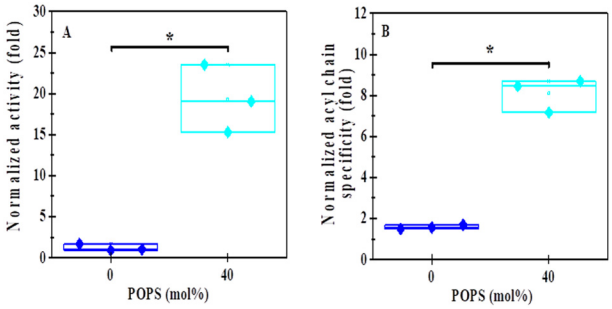

Figure 4. Membrane fusion intermediates enhances purified DGKε kinase activity and acyl-chain specificity. Liposomes composed of POPC/POPS/SAG ((90 − *x*):*x*:10; mol/mol/mol) were incubated in the absence and presence of 10 mM Ca^{2+} before activity assays. Normalized DGKε kinase activity (*A*) and acyl-chain specificity (*B*) are shown. Kinase activity and acyl-chain specificity (the ratio of SAG/DOG) were normalized to values in the absence of Ca^{2+}. These results were obtained using a final total lipid concentration of 5 mM at pH 7.2. Data are presented as a *box plot* including data of three independent experiments. *, $p < 0.01$.

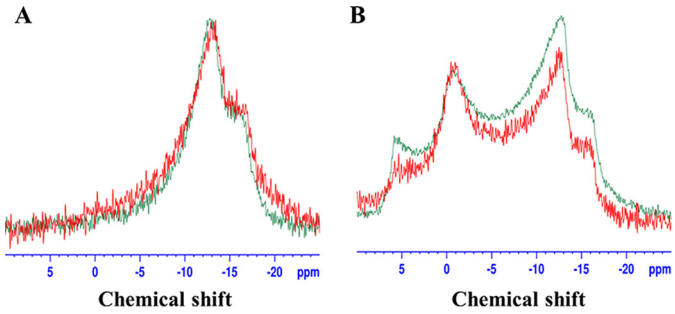

Figure 5. DGKε promotes membrane morphological changes. Shown are static ^{31}P NMR spectra of MLVs in solution bearing the phospholipid composition POPC/POPE/SAG (30:60:10; mol/mol/mol) (*A*) and DOPC/DOPE/SAG (30:60:10; mol/mol/mol) (*B*) in the absence (*green*) and presence (*red*) of DGKε. DGKε/lipid molar ratio was 1:10,000. Spectra were acquired at 25 °C. Experiments were carried out at pH 7.2. The spectra in the absence of DGKε (*green*) are reproduced from those shown in Fig. 2, *C* and *D*, respectively, to better visualize the effect of DGKε on the phase behavior of the lipid mixture.

relative to other phases. This effect was similarly observed either with SAG or DOG. It should also be noted that no ATP was added to the system, so that no reaction occurred, and no phosphatidic acid was formed during the NMR experiments. There were also no time-dependent changes in the spectral powder patterns. This finding of promotion of cubic phase formation has also been observed with viral fusion peptides/proteins (28, 31, 32), again linking cubic phases and membrane fusion.

Discussion

With regard to lipid signaling within a cell, inositol phospholipids are frequently cited due to their role in a variety of cell physiology phenomena (1, 2). In mammalian cells, inositol phospholipids are generally enriched with 1-stearoyl-2-arachidonoyl acyl-chains (6, 7). This acyl-chain enrichment is in part believed to be due to the action of DGKε, an enzyme of the PI cycle, the major metabolic pathway for the synthesis of inositol phospholipids. DGKε is the only mammalian isoform of DGK that has specificity for the acyl-chains of its substrates, a property that has been ascribed to an encoded motif in the enzyme (12). However, the current work clearly demonstrates that this acyl-chain specificity is not solely dependent on the structure of

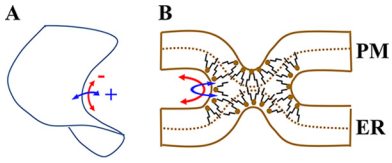

Figure 6. A *cartoon* depicting a saddle-like surface (*A*) and two membranes undergoing a fusion/fission event (*B*). Both of these structures present a negative Gaussian curvature (*i.e.* the principle curvatures at right angles present opposite signs as indicated by *blue* (positive curvature) and *red* (negative curvature) *arrows*). The positive curvature is in a plane orthogonal to the plane of the paper, and the negative curvature is in the plane of the paper.

the enzyme. By using a purified system with DGKε and model membranes, where we systematically varied the properties of the membranes, we identified highly curved membranes as the minimum requirement to activate the enzyme. Most importantly, the enzyme only showed enhanced acyl-chain specificity in systems with highly curved membranes. As DGKε lacks a putative regulatory domain, these data suggest that the enzyme is allosterically regulated by the curvature of the membrane to which the enzyme is bound as a major factor in controlling the activity and acyl-chain specificity of this enzyme. In the context of a cell, it is possible that there are additional factors resulting from the interaction of DGKε with other proteins or cofactors. When it comes to enzymatic catalysis at the membrane–water interface, the modulation of enzymatic activity at curved membranes could occur either by a preferential binding of the enzyme to the curved membrane, which enhances its local concentration without actually changing its specific enzyme activity, or by the curved membrane acting as an allosteric regulator of the enzyme (34). Our results clearly demonstrate that enzyme binding cannot explain the large difference observed between a locally flat (60% POPE) and highly curved membrane (60 mol % DOPE), supporting the conclusion that the enzyme is being allosterically regulated by the membrane curvature. These data suggest that within a cell, the enzyme works at a low basal level in locally flat membranes regardless of its lipid composition, and its function within the PI cycle is triggered by sites of highly curved membranes. For instance, in a cell, such highly curved membranes could be found at local sites where membrane fusion/fission takes place (Fig. 6).

There are many enzymes that function at membranes whose properties are modulated by membrane curvature (35–39). Membrane curvature can be broadly divided into two categories (*i.e.* intrinsic membrane curvature and physical membrane curvature). Intrinsic membrane curvature describes the tendency of a lipid or lipid mixture to form curved structures. It depends on the attractive and repulsive forces between lipid molecules (*i.e.* to the lateral pressure profile of the lipids) (40, 41). Several membrane-bound enzymes have their activity modulated by the intrinsic membrane curvature of the lipid molecules (35–39, 42–44). In contrast, the physical curvature of the membrane is simply its shape, independent of its lipid constituents (45). There are a variety of proteins that can sense and/or generate physical curvature (46). However, DGKε is unique in being allosterically regulated by the physical curvature of the membrane, but not by the intrinsic membrane curvature. Support for the statement that the intrinsic membrane

curvature has no effect comes from Fig. 2*A*, showing that the addition of DOPE, a lipid with strong intrinsic negative curvature, has no effect on activity up to 45 mol %, whereas the mixture is still a lamellar structure. In addition, Fig. 1*D* illustrates that a variety of lipids with different intrinsic curvatures, but all forming a lamellar structure, support similar activities of DGKε. On the other hand, DGKε activity is driven by the presence of highly curved membranes with lipids arranged in a nonlamellar structure. It is not only the enzyme activity that is driven by highly curved membranes but, most importantly, its substrate acyl-chain specificity.

In particular, we have identified two types of lipid structures that allosterically regulate the enzyme activity and acyl-chain specificity: the cubic phase and membrane fusion intermediates. Cubic phases in zwitterionic membranes and membrane fusion intermediates in PS-Ca^{2+} mixtures have little in common with each other, except that they both form similar kinds of highly bent structures (47, 48). These bent structures correspond to regions of certain cubic phases that allow the joining of one unit cell with another or, in the case of PS-Ca^{2+}, that forms the fusion pore between bilayers. These structures are described as having negative Gaussian curvature (*i.e.* a curvature, like a saddle point, in which the signs of the curvatures at right angles to each other are of opposite sign) (Fig. 6) (45). Many membrane active molecules can induce the formation of lipid structures with negative Gaussian curvature (28, 31, 32). Based on the ^{31}P NMR evidence, DGKε also favors the formation of these structures. However, to our knowledge, there has not been any report in the literature of the activity of an enzyme being allosterically regulated by this kind of curvature, which makes DGKε unique in that regard. It is noteworthy that it is not only DGKε activity that is allosterically regulated by this kind of curvature, but also its substrate acyl-chain specificity, an important property of the enzyme to function within the PI cycle. Gaussian curvature is known to be required for the formation of membrane fusion/fission intermediates, and it must be present in living cells at sites of membrane fusion/fission as well as other locations where planar bilayers are greatly affected by curvature (49). This level of mechanistic insight would not be possible to demonstrate without the use of a cell-free system, as there are at least 10 known diacylglycerol kinase isoforms with currently no isoform-specific inhibitor. In addition, membranes with negative Gaussian curvature represent a small fraction of biological membranes and usually are formed in highly dynamic processes like membrane trafficking or fusion/fission events.

The PI cycle plays a role in several cell physiology phenomena (1, 2). Of particular importance for the present study is membrane trafficking. Recent studies indicate a role played by DAG and PA in the regulation of membrane trafficking, which suggests that DGK can also play a role in this biological function (50). Of all mammalian DGK isoforms, DGKε is the one with the greatest likelihood to mediate membrane trafficking due to its role in the PI cycle. In the membrane-trafficking pathway, two morphologically similar, but oppositely ordered, membrane rearrangements take place: membrane fusion and fission (51). It is interesting to note that membrane fusion intermediates are sites of maximum DGKε kinase activity and acyl-chain specificity. Hence, our data suggest that DGKε plays a role in membrane trafficking, shedding light on a proposed new biological function of DGKε.

In the PI cycle, reactions take place in two membranes (*i.e.* the PM and ER, which are the membranes where DGKε has been reported to be found) (13, 14). For proper cycle function, lipid intermediates need to be transported from one membrane to another in both directions. In particular, the movement of DAG and PA has been reported to occur through specific lipid carrier proteins that co-localize with PM–ER contact sites (52). It is now becoming more evident that contact sites between membranes, where two distinct membranes are in close proximity to each other (~10–30 nm), within the cell are more common than first anticipated, including the presence of PM–ER contact sites (52–54). PM–ER contact sites can adopt distinct shapes in a cell-specific manner or even within a cell type (55–59). In addition, even for contact sites between the same two organelles, there can be sites containing different proteins and, therefore, having different functions (57). For instance, only some of the contact sites between the ER and PM are enriched in the protein GRAMD2a (57). GRAMD2a associates with PI lipids, and these contact sites are found at sites enriched in phosphatidylinositol 4,5-bisphosphate, suggesting that this contact site may be involved in the PI cycle. It is thus likely that DGKε is present in these contact sites, which would locate the protein in a suitable environment to trigger its activity and acyl-chain specificity upon membrane morphological changes, tightly regulating the PI cycle. This proposition is consistent with the observation that in a biological membrane, DGKε is not randomly distributed in the membrane but rather is present in discrete locations close to the PM (60, 61). In the basal state, DGKε would have low activity and low acyl-chain specificity, but upon stimulation, the enzyme would be activated at specific sites of the membrane having high negative Gaussian curvature. This activation would be transient.

By employing a cell-free system, we were able to show that DGKε can be regulated only by the nature of the membrane it is bound to, specifically the shape of the membrane. To our knowledge, this mode of regulation of an enzyme's activity by the actual shape of the membrane to which it is bound, rather than to intrinsic membrane curvature, is the first example of such a regulatory mechanism. In membranes that present negative Gaussian curvature, the enzyme is activated as well as being able to differentiate the nature of the acyl-chains of its lipid substrate, an important property for its function within the PI cycle. In a fine-tune interplay with the membrane, DGKε is not only allosterically regulated by the shape of the membrane it is bound to, but it also promotes the formation of curved membranes in systems that have the propensity to form those structures. These findings suggest that in a cellular context, DGKε is functioning at a very low basal activity to catalyze the conversion of DAG to PA without acyl-chain discrimination in a locally flat region of the membrane. However, the enzyme actively engages in the PI cycle upon membrane global morphological changes, with a great likelihood of the enzyme playing a role in membrane trafficking. It is likely that in a cell environment, this regulation will be modified by other molecular components including proteins, other lipids, etc.

However, in addition to these modulating factors, the study described here demonstrates that a major regulatory factor is the shape of the membrane to which the enzyme binds. This type of enzyme regulation comes to light as a new, complementary, and synergistic mechanism for the regulation of membrane signaling phenomena.

Experimental procedures

Materials

All lipids used in this study were purchased from Avanti Polar Lipids (Alabaster, AL). Ni-NTA–agarose resin was from Qiagen (Germany). [γ-^{32}P]ATP was purchased from Perkin-Elmer Life Sciences. All reagents were used as received.

DGKϵ overexpression and purification

Human full-length DGKϵ-His_6 was overexpressed in Sf21 insect cells using recombinant baculovirus for cell infection as described by Jennings *et al.* (62). Enzyme was affinity-purified with Ni-NTA resin. Initial experiments were conducted using the purification procedure described by Jennings *et al.* (62); however, most of the studies used a slightly different protocol for enzyme purification, which yielded a more stable form of the purified enzyme upon freezing at −80 °C for storage. Briefly, cell pellets overexpressing the enzyme were lysed using lysis buffer (20 mM Tris-HCl, pH 8, 500 mM NaCl, 20% (v/v) glycerol, 10 mM imidazole, 1 mM β-glycerophosphate, 1 mM activated sodium orthovanadate, 2.5 mM sodium pyrophosphate, a 1:1,000 dilution of Roche protease inhibitor mixture tablet in water, 2% (v/v) Triton X-100, 0.05% (v/v) β-mercaptoethanol), and the obtained lysate was clarified by centrifuging it at 13,000 × *g* for 30 min at 4 °C. The clarified lysate was incubated with Ni-NTA resin at a ratio of 15:1 for 1 h on an inverting rotor at 4 °C. Following the binding step, the resin was washed three times for 5 min each time with wash buffer (20 mM Tris-HCl, pH 8.0, 500 mM NaCl, 20% (v/v) glycerol, 30 mM imidazole, 0.05% (v/v) Tween 20, 0.05% (v/v) β-mercaptoethanol) on an inverting rotor at 4 °C. Purified enzyme was eluted using elution buffer (20 mM Tris-HCl, pH 8.0, 500 mM NaCl, 20% (v/v) glycerol, 300 mM imidazole, 0.05% (v/v) Tween 20, 0.05% β-mercaptoethanol) on an inverting rotor at 4 °C for 10 min and either used fresh for the experiments or flash-frozen with liquid nitrogen and stored at −80 °C.

Model membrane preparation

Lipids stock solutions were prepared from powder in chloroform/methanol (2:1) (v/v). The concentration of the phospholipids was determined by measuring the amount of P_i released after digestion by the method of Ames (63). Lipids at the desired molar ratio were deposited as a film on the wall of a glass test tube by solvent evaporation under a nitrogen flux. Final traces of solvent were removed for 2–3 h in a vacuum chamber attached to a liquid nitrogen trap. The lipid films were then suspended in liposome buffer (10 mM HEPES, 100 mM NaCl, pH 7.2) or 4× mixed micelle buffer (200 mM MOPS, 400 mM NaCl, 20 mM $MgCl_2$, 4 mM EGTA, 1 mM DTT, 60 mM Triton X-100, pH 7.2) by vortexing at room temperature to form MLVs or mixed micelles, respectively. LUVs were prepared by processing MLVs with 10 passages through two stacked polycarbonate membranes (100- or 200-nm pore size; Nucleopore Filtration Products, Pleasanton, CA) in a barrel extruder (Lipex Biomembranes). Small unilamellar vesicles were prepared by sonicating MLVs in a Cole–Palmer bath type ultrasonic cleaner, model 08849-00, until a clear solution was obtained. Model membranes were used for experimentation right after preparation. The lipid compositions of ER and PM model membranes were, respectively, POPC/POPE/liver PI/POPS/cholesterol/DAG (40:22:12:4:12:10; mol %) and POPC/POPE/liver PI/POPS/ SM/cholesterol/DAG (18:11:1:3:12:45:10; mol %).

DLS

The hydrodynamic size of the model membranes was determined by DLS measurements using a Zetasizer Nano S system (Malvern Panalytical, Malvern, UK). The measurements were done at 20 °C.

Kinase activity assays

Activity assays were performed using methods described previously (62). Briefly, the reaction mixture containing 50 μl of 20 mM model membranes, 50 μl of assay buffer (50 mM HEPES, 300 mM NaCl, 20 mM $MgCl_2$, 4 mM EGTA, pH 7.2) or ddH_2O (for mixed micelles), 20 μl of 10 mM dithiothreitol, and 35 μl of ddH_2O were added to a silanilized glass tube. Then 25 μl of purified DGKϵ was added to the reaction mixture and incubated for 10 min at 20 °C. The reaction was started by adding 20 μl of 5 mM ATP in the presence of trace amounts of [γ-^{32}P]ATP (50 μCi ml^{-1}). All reactions were performed using a 10-min end point at 20 °C, after which the reaction was quenched with 2 ml of stop solution (1:1 (v/v) chloroform/methanol, 0.25 mg ml^{-1} dihexadecylphosphate). The organic phase was washed three times with 2 ml of wash solution (7:1 ddH_2O/CH_3OH, 1% $HClO_4$, 100 mM H_3PO_4). The radioactivity of the organic-soluble phase was measured using a liquid scintillation counter (Beckman Coulter). All experiments were conducted within the linear range of enzyme activity in regard to its amount and incubation time (not shown).

Enzyme specific activity was calculated using Equation 1,

$$\text{Specific activity} = \frac{(R-B)\times\dfrac{(n_{ATP})}{(P-B)}\times f_{org}}{(t\times m_{DGK\epsilon})} \quad \text{(Eq. 1)}$$

where R, B, and P are the raw counts of the sample, background, and positive control, respectively. n_{ATP} is the mol of ATP used on the reaction mixture, f_{org} is the volume fraction of organic phase used to measure the radioactivity, t is the time of reaction, and $m_{DGK\epsilon}$ is the mass of DGKϵ in the reaction mixture.

To obtain the kinetic parameters K_m and V_{max}, the data set was fitted using Equation 2,

$$\text{Specific activity} = \frac{V_{max}\times[S]}{K_m+[S]} \quad \text{(Eq. 2)}$$

where V_{max}, $[S]$, and K_m are, respectively, the maximum reaction rate, substrate mol %, and the K_m.

Binding assay

The fraction of liposome-bound DGKϵ was quantified by an ultracentrifugation assay. Briefly, DGKϵ and MLVs of the desired lipid composition were incubated for 10 min at 20 °C in the same reaction mixture as per the activity assay but without the addition of ATP. A small aliquot (100 μl) of the mixture was saved as the input (or total amount of protein), and the unbound enzyme was removed by ultracentrifugation (100,000 × *g* for 1 h at 20 °C). Pellets were resuspended in assay buffer. The fraction of proteins bound to liposomes was analyzed by immunoblotting as the ratio between pellet and input.

Immunoblotting

Western blots were conducted to quantify purified enzyme for the calculation of its specific activity and binding to liposomes. To ensure the quantification was performed within the dynamic range of the assay, first a serial dilution of purified enzyme was conducted, and, when needed, a dilution of the sample was conducted before quantification. Briefly, samples were separated in 7.5% hand-cast polyacrylamide gels and transferred to polyvinylidene difluoride membranes (0.2 μm; Bio-Rad). Immunoblotting was performed with a mouse anti-His tag antibody (Abcam). Secondary antibodies coupled to horseradish peroxidase were used to detect the bands using a homemade ECL reagent. Densitometric analysis of the bands was performed using ImageJ. For the quantification of the enzyme for the calculation of specific activity, a purified His-tagged protein (DAHP synthase) of known concentration was used as a standard.

^{31}P NMR

The ^{31}P NMR spectra, from a 65 mM concentration of the desired lipid mixture or a 33 mM concentration of lipids in the presence of DGKϵ in 10 mM HEPES, 100 mM NaCl, pH 7.2, were obtained using a Bruker AVIII 700-MHz spectrometer equipped with a 5 mm QNP cryoprobe over 17-kHz sweep width in 32,768 data points. The sample was contained in a 5-mm diameter Shigemi NMR tube (Shigemi Co., Tokyo, Japan). Block decay spectra were acquired using a 30° pulse, inverse gated proton decoupling, and 2-s total recycle time. Unless otherwise indicated, all NMR spectra were recorded at a 25 °C sample temperature. The spectra were generated by Fourier transform of the first 1024 free induction decay data points and zero-filled to 8192 points.

X-ray diffraction

Small-angle X-ray diffraction measurements were conducted according to previously published procedures (64). Briefly, 65 mM lipid (DOPC/DOPE/SAG, 30:60:10; mol %) was prepared as MLVs in 10 mM HEPES, 100 mM NaCl, pH 7.2, heated at 70 °C for 10 min, gently centrifuged into a single pellet, which was applied on a silicon wafer. The chip was annealed for 1 day at 38 °C and 100% relative humidity and measured in a chamber at 30 °C and 97% relative humidity. X-ray scattering data were acquired using the Biological Large Angle Diffraction Experiment (BLADE), a CuKα Rigaku Smartlab rotating anode at 1.5418-Å wavelength using 9 kilowatts (45 kV, 200 mA) and a HyPix-3000 hybrid pixel array detector.

To calculate the radius of the water channels in the Pn3m cubic phase, we used the equation described by Tyler *et al.* (65),

$$r_w = 0.391 \times a - l \quad \text{(Eq. 3)}$$

where r_W, a, and l are radius of the water channel, the lattice parameter, and the monolayer thickness (here assumed to be 19 Å according to Ding *et al.* (33)), respectively.

Statistical analysis

A two-tailed *t* test was used for all of the statistical analysis in this work.

Author contributions—J. C. B., W. J., S. B., Y. H. H., D. L., and P. C. conducted and analyzed kinase activity assays. J. C. B. and W. J. conducted and analyzed binding assays. Y. H. H. performed DLS measurements. J. C. B., B. B., and T. K. performed ^{31}P NMR measurements. A. K. and M. R. conducted X-ray diffraction measurements. J. C. B. and R. M. E. designed the experiments, analyzed the data, and wrote the manuscript. R. M. E. provided materials and laboratory facilities.

Acknowledgments—We thank Dr. P. J. Bert and Dr. M. Heimhalt for providing purified His-tagged DAHP synthase used in this work as a standard for DGKϵ quantification and Dr. David Siegel for helpful discussions.

References

1. Di Paolo, G., and De Camilli, P. (2006) Phosphoinositides in cell regulation and membrane dynamics. *Nature* **443,** 651–657 CrossRef Medline
2. Balla, T. (2013) Phosphoinositides: tiny lipids with giant impact on cell regulation. *Physiol. Rev.* **93,** 1019–1137 CrossRef Medline
3. Rohács, T., Chen, J., Prestwich, G. D., and Logothetis, D. E. (1999) Distinct specificities of inwardly rectifying K^+ channels for phosphoinositides. *J. Biol. Chem.* **274,** 36065–36072 CrossRef Medline
4. Cho, H., and Kim, Y. A., Ho, W.-K. (2006) Phosphate number and acyl chain length determine the subcellular location and lateral mobility of phosphoinositides. *Mol. Cells* **22,** 97–103 Medline
5. Doignon, F., Laquel, P., Testet, E., Tuphile, K., Fouillen, L., and Bessoule, J.-J. (2015) Requirement of phosphoinositides containing stearic acid to control cell polarity. *Mol. Cell Biol.* **36,** 765–780 CrossRef Medline
6. Bone, L. N., Dayam, R. M., Lee, M., Kono, N., Fairn, G. D., Arai, H., Botelho, R. J., and Antonescu, C. N. (2017) The acyltransferase LYCAT controls specific phosphoinositides and related membrane traffic. *Mol. Biol. Cell* **28,** 161–172 CrossRef Medline
7. Mujalli, A., Chicanne, G., Bertrand-Michel, J., Viars, F., Stephens, L., Hawkins, P., Viaud, J., Gaits-Iacovoni, F., Severin, S., Gratacap, M. P., Terrisse, A. D., and Payrastre, B. (2018) Profiling of phosphoinositide molecular species in human and mouse platelets identifies new species increasing following stimulation. *Biochim. Biophys. Acta Mol. Cell Biol. Lipids.* **1863,** 1121–1131 CrossRef Medline
8. Kimura, T., Jennings, W., and Epand, R. M. (2016) Roles of specific lipid species in the cell and their molecular mechanism. *Prog. Lipid Res.* **62,** 75–92 CrossRef Medline
9. Rodriguez de Turco, E. B., Tang, W., Topham, M. K., Sakane, F., Marcheselli, V. L., Chen, C., Taketomi, A., Prescott, S. M., and Bazan, N. G. (2001) Diacylglycerol kinase ϵ regulates seizure susceptibility and long-term potentiation through arachidonoyl-inositol lipid signaling. *Proc. Natl. Acad. Sci. U.S.A.* **98,** 4740–4745 CrossRef Medline
10. Milne, S. B., Ivanova, P. T., Armstrong, M. D., Myers, D. S., Lubarda, J., Shulga, Y. V., Topham, M. K., Brown, H. A., and Epand, R. M. (2008) Dramatic differences in the roles in lipid metabolism of two isoforms of diacylglycerol kinase. *Biochemistry* **47,** 9372–9379 CrossRef Medline

11. Tang, W., Bunting, M., Zimmerman, G. A., McIntyre, T. M., and Prescott, S. M. (1996) Molecular cloning of a novel human diacylglycerol kinase highly selective for arachidonate-containing substrates. *J. Biol. Chem.* **271,** 10237–10241 CrossRef Medline
12. Shulga, Y. V., Topham, M. K., and Epand, R. M. (2011) Study of arachidonoyl specificity in two enzymes of the PI cycle. *J. Mol. Biol.* **409,** 101–112 CrossRef Medline
13. Kobayashi, N., Hozumi, Y., Ito, T., Hosoya, T., Kondo, H., and Goto, K. (2007) Differential subcellular targeting and activity-dependent subcellular localization of diacylglycerol kinase isozymes in transfected cells. *Eur. J. Cell Biol.* **86,** 433–444 CrossRef Medline
14. Decaffmeyer, M., Shulga, Y. V., Dicu, A. O., Thomas, A., Truant, R., Topham, M. K., Brasseur, R., and Epand, R. M. (2008) Determination of the topology of the hydrophobic segment of mammalian diacylglycerol kinase ε in a cell membrane and its relationship to predictions from modeling. *J. Mol. Biol.* **383,** 797–809 CrossRef Medline
15. Natalini, P. M., Zulian, S. E., Ilincheta de Boschero, M. G., and Giusto, N. M. (2013) Diacylglycerol kinase ε in bovine and rat photoreceptor cells: light-dependent distribution in photoreceptor cells. *Exp. Eye Res.* **112,** 139–150 CrossRef Medline
16. Sato, Y., Murakami, C., Yamaki, A., Mizuno, S., Sakai, H., and Sakane, F. (2016) Distinct 1-monoacylglycerol and 2-monoacylglycerol kinase activities of diacylglycerol kinase isozymes. *Biochim. Biophys. Acta* **1864,** 1170–1176 CrossRef Medline
17. Epand, R. M., and Topham, M. K. (2007) Measurement of mammalian diacylglycerol kinase activity *in vitro* and in cells. *Methods Enzymol.* **434,** 293–304 CrossRef Medline
18. D'Souza, K., and Epand, R. M. (2012) Catalytic activity and acyl-chain selectivity of diacylglycerol kinase ε are modulated by residues in and near the lipoxygenase-like motif. *J. Mol. Biol.* **416,** 619–628 CrossRef Medline
19. van Meer, G., Voelker, D. R., and Feigenson, G. W. (2008) Membrane lipids: where they are and how they behave. *Nat. Rev. Mol. Cell Biol.* **9,** 112–124 CrossRef Medline
20. Kollmitzer, B., Heftberger, P., Rappolt, M., and Pabst, G. (2013) Monolayer spontaneous curvature of raft-forming membrane lipids. *Soft Matter* **9,** 10877–10884 CrossRef Medline
21. Marsh, D. (2007) Lateral pressure profile, spontaneous curvature frustration, and the incorporation and conformation of proteins in membranes. *Biophys. J.* **93,** 3884–3899 CrossRef Medline
22. Rappolt, M., Hickel, A., Bringezu, F., and Lohner, K. (2003) Mechanism of the lamellar/inverse hexagonal phase transition examined by high resolution x-ray diffraction. *Biophys. J.* **84,** 3111–3122 CrossRef Medline
23. Cullis, P. R., and de Kruijff, B. (1979) Lipid polymorphism and the functional roles of lipids in biological membranes. *Biochim. Biophys. Acta* **559,** 399–420 CrossRef Medline
24. Goñi, F. M., and Alonso, A. (1999) Structure and functional properties of diacylglycerols in membrane. *Prog. Lipid Res.* **38,** 1–48 CrossRef Medline
25. Nieva, J. L., Alonso, A., Basáñez, G., Goñi, F. M., Gulik, A., Vargas, R., and Luzzati, V. (1995) Topological properties of 2 cubic phases of a phospholipid-cholesterol-diacylglycerol aqueous system and their possible implications in the phospholipase C-induced liposome fusion. *FEBS Lett.* **368,** 143–147 CrossRef Medline
26. Demurtas, D., Guichard, P., Martiel, I., Mezzenga, R., Hébert, C., and Sagalowicz, L. (2015) Direct visualization of dispersed lipid bicontinuous cubic phases by cryo-electron tomography. *Nat. Commun.* **6,** 8915 CrossRef Medline
27. Luzzati, V. (1997) Biological significance of lipid polymorphism: the cubic phases. *Curr. Opin. Struct. Biol.* **7,** 661–668 CrossRef Medline
28. Yao, H., Lee, M. W., Waring, A. J., Wong, G. C. L., and Hong, M. (2015) Viral fusion protein transmembrane domain adopts β-strand structure to facilitate membrane topological changes for virus–cell fusion. *Proc. Natl. Acad. Sci. U.S.A.* **112,** 10926–10931 CrossRef Medline
29. Rand, R. P., Kachar, B., and Reese, T. S. (1985) Dynamic morphology of calcium-induced interactions between phosphatidylserine vesicles. *Biophys. J.* **47,** 483–489 CrossRef Medline
30. Düzgüneş, N., Wilschut, J., Hong, K., Fraley, R., Perry, C., Friend, D. S., James, T. L., and Papahadjopoulos, D. (1983) Physicochemical characterization of large unilamellar phospholipid vesicles prepared by reverse-phase evaporation. *Biochim. Biophys. Acta* **732,** 289–299 CrossRef Medline
31. Fuhrmans, M., Knecht, V., and Marrink, S. J. (2009) A single bicontinuous cubic phase induced by fusion peptides. *J. Am. Chem. Soc.* **131,** 9166–9167 CrossRef Medline
32. Colotto, A., Martin, I., Ruysschaert, J. M., Sen, A., Hui, S. W., and Epand, R. M. (1996) Structural study of the interaction between the SIV fusion peptide and model membranes. *Biochemistry* **35,** 980–989 CrossRef Medline
33. Ding, W., Palaiokostas, M., Wang, W., and Orsi, M. (2015) Effects of lipid composition on bilayer membranes quantified by all-atom molecular dynamics. *J. Phys. Chem. B* **119,** 15263–15274 CrossRef Medline
34. Iversen, L., Mathiasen, S., Larsen, J. B., and Stamou, D. (2015) Membrane curvature bends the laws of physics and chemistry. *Nat. Chem. Biol.* **11,** 822–825 CrossRef Medline
35. Attard, G. S., Templer, R. H., Smith, W. S., Hunt, A. N., and Jackowski, S. (2000) Modulation of CTP:phosphocholine cytidylyltransferase by membrane curvature elastic stress. *Proc. Natl. Acad. Sci. U.S.A.* **97,** 9032–9036 CrossRef Medline
36. Andersen, O. S., and Koeppe, R. E., 2nd (2007) Bilayer thickness and membrane protein function: an energetic perspective. *Annu. Rev. Biophys. Biomol. Struct.* **36,** 107–130 CrossRef Medline
37. Phillips, R., Ursell, T., Wiggins, P., and Sens, P. (2009) Emerging roles for lipids in shaping membrane-protein function. *Nature* **459,** 379–385 CrossRef Medline
38. Soubias, O., Teague, W. E., Jr., Hines, K. G., Mitchell, D. C., and Gawrisch, K. (2010) Contribution of membrane elastic energy to rhodopsin function. *Biophys. J.* **99,** 817–824 CrossRef Medline
39. Schlame, M., Acehan, D., Berno, B., Xu, Y., Valvo, S., Ren, M., Stokes, D. L., and Epand, R. M. (2012) The physical state of lipid substrates provides transacylation specificity for tafazzin. *Nat. Chem. Biol.* **8,** 862–869 CrossRef Medline
40. Brown, M. F. (2012) Curvature forces in membrane lipid–protein interactions. *Biochemistry* **51,** 9782–9795 CrossRef Medline
41. Cantor, R. S. (1997) The lateral pressure profile in membranes: a physical mechanism of general anesthesia. *Biochemistry* **36,** 2339–2344 CrossRef Medline
42. Li, M., Khan, S., Rong, H., Tuma, R., Hatzakis, N. S., and Jeuken, L. J. C. (2017) Effects of membrane curvature and pH on proton pumping activity of single cytochrome bo3 enzymes. *Biochim. Biophys. Acta Bioenerg.* **1858,** 763–770 CrossRef Medline
43. Haider, A., Wei, Y.-C., Lim, K., Barbosa, A. D., Liu, C.-H., Weber, U., Mlodzik, M., Oras, K., Collier, S., Hussain, M. M., Dong, L., Patel, S., Alvarez-Guaita, A., Saudek, V., Jenkins, B. J., *et al.* (2018) PCYT1A regulates phosphatidylcholine homeostasis from the inner nuclear membrane in response to membrane stored curvature elastic stress. *Dev. Cell* **45,** 481–495.e8 CrossRef Medline
44. Renne, M. F., and de Kroon, A. I. P. M. (2018) The role of phospholipid molecular species in determining the physical properties of yeast membranes. *FEBS Lett.* **592,** 1330–1345 CrossRef Medline
45. Zimmerberg, J., and Kozlov, M. M. (2006) How proteins produce cellular membrane curvature. *Nat. Rev. Mol. Cell Biol.* **7,** 9–19 CrossRef Medline
46. Jarsch, I. K., Daste, F., and Gallop, J. L. (2016) Membrane curvature in cell biology: an integration of molecular mechanisms. *J. Cell Biol.* **214,** 375–387 CrossRef Medline
47. Salditt, T., and Aeffner, S. (2016) X-ray structural investigations of fusion intermediates: lipid model systems and beyond. *Semin. Cell Dev. Biol.* **60,** 65–77 CrossRef Medline
48. Graber, Z. T., Shi, Z., and Baumgart, T. (2017) Cations induce shape remodeling of negatively charged phospholipid membranes. *Phys. Chem. Chem. Phys.* **19,** 15285–15295 CrossRef Medline
49. Almsherqi, Z. A., Landh, T., Kohlwein, S. D., and Deng, Y. (2009) Chapter 6: Cubic membranes: the missing dimension of cell membrane organization. *Int. Rev. Cell Mol. Biol.* **274,** 275–342 CrossRef Medline
50. Xie, S., Naslavsky, N., and Caplan, S. (2015) Diacylglycerol kinases in membrane trafficking. *Cell. Logist.* **5,** e1078431 CrossRef Medline

51. McMahon, H. T., and Gallop, J. L. (2005) Membrane curvature and mechanisms of dynamic cell membrane remodelling. *Nature* **438,** 590–596 CrossRef Medline
52. Saheki, Y., and De Camilli, P. (2017) Endoplasmic reticulum–plasma membrane contact sites. *Annu. Rev. Biochem.* **86,** 659–684 CrossRef Medline
53. Shai, N., Yifrach, E., van Roermund, C. W. T., Cohen, N., Bibi, C., IJlst, L., Cavellini, L., Meurisse, J., Schuster, R., Zada, L., Mari, M. C., Reggiori, F. M., Hughes, A. L., Escobar-Henriques, M., Cohen, M. M., *et al.* (2018) Systematic mapping of contact sites reveals tethers and a function for the peroxisome-mitochondria contact. *Nat. Commun.* **9,** 1761 CrossRef Medline
54. Bohnert, M., and Schuldiner, M. (2018) Stepping outside the comfort zone of membrane contact site research. *Nat. Rev. Mol. Cell Biol.* **19,** 483–484 CrossRef
55. Lees, J. A., Messa, M., Sun, E. W., Wheeler, H., Torta, F., Wenk, M. R., De Camilli, P., and Reinisch, K. M. (2017) Lipid transport by TMEM24 at ER-plasma membrane contacts regulates pulsatile insulin secretion. *Science* **355,** eaah6171 CrossRef Medline
56. Klausner, R. D., Donaldson, J. G., and Lippincott-Schwartz, J. (1992) Brefeldin A: insights into the control of membrane traffic and organelle structure. *J. Cell Biol.* **116,** 1071–1080 CrossRef Medline
57. Besprozvannaya, M., Dickson, E., Li, H., Ginburg, K. S., Bers, D. M., Auwerx, J., and Nunnari, J. (2018) GRAM domain proteins specialize functionally distinct ER-PM contact sites in human cells. *Elife* **7,** e31019 Medline
58. Salvador-Gallego, R., Hoyer, M. J., and Voeltz, G. K. (2017) SnapShot: functions of endoplasmic reticulum membrane contact sites. *Cell* **171,** 1224–1224.e1 CrossRef Medline
59. Stefan, C. J., Manford, A. G., and Emr, S. D. (2013) ER-PM connections: sites of information transfer and inter-organelle communication. *Curr. Opin. Cell Biol.* **25,** 434–442 CrossRef Medline
60. Hozumi, Y., Akimoto, R., Suzuki, A., Otani, K., Watanabe, M., and Goto, K. (2015) Expression and localization of the diacylglycerol kinase family and of phosphoinositide signaling molecules in adrenal gland. *Cell Tissue Res.* **362,** 295–305 CrossRef Medline
61. Hozumi, Y., Fujiwara, H., Kaneko, K., Fujii, S., Topham, M. K., Watanabe, M., and Goto, K. (2017) Diacylglycerol kinase ϵ localizes to subsurface cisterns of cerebellar Purkinje cells. *Cell Tissue Res.* **368,** 441–458 CrossRef Medline
62. Jennings, W., Doshi, S., Hota, P. K., Prodeus, A., Black, S., and Epand, R. M. (2017) Expression, purification, and properties of a human arachidonoyl-specific isoform of diacylglycerol kinase. *Biochemistry* **56,** 1337–1347 CrossRef Medline
63. Ames, B. N. (1966) Assay of inorganic phosphate, total phosphate and phosphatases. *Methods Enzymol.* **8,** 115–118 CrossRef
64. Khondker, A., Malenfant, D. J., Dhaliwal, A. K., and Rheinstädter, M. C. (2018) Carbapenems and lipid bilayers: localization, partitioning, and energetics. *ACS Infect. Dis.* **4,** 926–935 CrossRef Medline
65. Tyler, A. I. I., Barriga, H. M. G., Parsons, E. S., McCarthy, N. L. C., Ces, O., Law, R. V., Seddon, J. M., and Brooks, N. J. (2015) Electrostatic swelling of bicontinuous cubic lipid phases. *Soft Matter* **11,** 3279–3286 CrossRef Medline

Membrane curvature allosterically regulates the phosphatidylinositol cycle, controlling its rate and acyl-chain composition of its lipid intermediates

José Carlos Bozelli Jr., William Jennings, Stephanie Black, Yu Heng Hou, Darius Lameire, Preet Chatha, Tomohiro Kimura, Bob Berno, Adree Khondker, Maikel C. Rheinstädter and Richard M. Epand

J. Biol. Chem. 2018, 293:17780-17791.
doi: 10.1074/jbc.RA118.005293 originally published online September 20, 2018
